Title: Inhalable polymer nanoparticles for versatile mRNA delivery and mucosal vaccination

Authors: Alexandra Suberi[1], Molly K. Grun[2], Tianyang Mao[3], Benjamin Israelow[3,4], Melanie Reschke[5], Julian Grundler[6], Laiba Akhtar[2], Teresa Lee[1], Kwangsoo Shin[1], Alexandra S. Piotrowski-Daspit[1], Robert J. Homer[7], Akiko Iwasaki[3,8], Hee Won Suh[1*], W. Mark Saltzman[1,2,9*]

Affiliations:
[1]Department of Biomedical Engineering, Yale University, New Haven, CT, USA
[2]Department of Chemical & Environmental Engineering, Yale University, New Haven, CT, USA
[3]Department of Immunobiology, Yale University School of Medicine, New Haven, CT, USA
[4]Department of Medicine, Section of Infectious Diseases, Yale University School of Medicine, New Haven, CT, USA
[5]Department of Molecular Biophysics and Biochemistry, Yale University, New Haven, CT, USA
[6]Department of Chemistry, Yale University, New Haven, CT, USA
[7]Department of Pathology, Yale University School of Medicine, CT, USA
[8]Howard Hughes Medical Institute, Chevy Chase, MD, USA
[9]Department of Cellular & Molecular Physiology, Yale School of Medicine, New Haven, CT, USA

*Corresponding authors. Email: heewon.suh@yale.edu and mark.saltzman@yale.edu

Abstract (125 words):
An inhalable platform for mRNA therapeutics would enable minimally invasive and lung targeted delivery for a host of pulmonary diseases. Development of lung targeted mRNA therapeutics has been limited by poor transfection efficiency and risk of vehicle-induced pathology. Here we report an inhalable polymer-based vehicle for delivery of therapeutic mRNAs to the lung. We optimized biodegradable poly(amine-co-ester) polyplexes for mRNA delivery using end group modifications and polyethylene glycol. Our polyplexes achieved high transfection of mRNA throughout the lung, particularly in epithelial and antigen-presenting cells. We applied this technology to develop a mucosal vaccine for SARS-CoV-2. Intranasal vaccination with spike protein mRNA polyplexes induced potent cellular and humoral adaptive immunity and protected K18-hACE2 mice from lethal viral challenge.

One-sentence summary:
Inhaled polymer nanoparticles (NPs) achieve high mRNA expression in the lung and induce protective immunity against SARS-CoV-2.

Main Text:

mRNA-based vaccines for SARS-CoV-2 have demonstrated the enormous potential of mRNA therapeutics for safe and effective use in the general population (1, 2). The long-anticipated development of mRNA vaccines was enabled by critical advancements in mRNA technology that improved stability and transfection while minimizing innate immune activation (3). To capitalize on these advancements, and expand the application of mRNA therapeutics beyond delivery of systemically administered vaccines, further research and development is required to optimize mRNA delivery vehicles for diverse applications *in vivo* (4, 5). In particular, inhalable mRNA delivery vehicles would enable minimally invasive and lung targeted therapies for pulmonary diseases. Inhaled delivery would be ideal for creating improved mucosal vaccines for respiratory pathogens, protein supplementation, or gene editing in the lung (6-9). However, the lipid nanoparticle (LNP) materials that are currently used for intramuscular mRNA SARS-CoV-2 vaccines are not easily adapted for inhalation delivery (10).

Several major limitations have hindered the development of inhaled mRNA therapeutics. First, mRNA delivery vehicle efficacy is highly dependent on the route of administration (11) and must therefore be optimized for expression in the lung. High transfection efficiency is required to reduce the therapeutic dose and reach the concentration of protein necessary to achieve a therapeutic response. For example, despite initially promising safety and tolerability, RESTORE-CF—an ongoing inhaled mRNA clinical trial, delivering CFTR mRNA in LNPs for treatment of cystic fibrosis— failed to improve pulmonary function in the second interim report, highlighting the need for improvements in the delivery vehicle (12). Another key concern for inhaled therapeutic delivery is that the respiratory mucosa is particularly susceptible to immunopathology (13). Several components of the LNP delivery vehicles used in both approved mRNA vaccines have been shown to induce inflammation in the respiratory tract after intranasal administration (10). A NP optimized for inhaled administration that achieves high mRNA transfection efficiency without inducing an inflammatory immune response that damages the lungs, is needed to enable development of pulmonary mRNA therapeutics.

We sought to overcome the challenges to delivering inhaled mRNA by creating an inhalable, non-inflammatory, polymer-based delivery vehicle. Previously, we have demonstrated that a family of nontoxic biodegradable poly(amine-co-ester) (PACE) polymers can encapsulate and protect nucleic acid cargos for delivery *in vivo* (14). The chemical composition of PACE polymers is highly tunable depending on the monomer components added to the polymerization reaction, the ratios of the components, and synthesis conditions (15). For certain polymer compositions, PACE polymers form polyplexes with mRNA (PACE-mRNA) through a combination of electrostatic interactions between the mildly cationic polymer and the negatively charged phosphate backbone of nucleic acids as well as hydrophobic interactions between segments of the polymer chain. PACE polymers can also be modified through the addition of end groups. We have demonstrated that amine containing end groups can improve transfection efficiency by facilitating endosomal escape of mRNA from the endocytosed NP into the cytoplasm (16). Stabilization of PACE-mRNA polyplexes with polyethylene glycol (PEG) can further improve mRNA delivery *in vivo* (17). We capitalized on the highly tunable nature of PACE polyplexes by screening a library of delivery vehicles with different chemical end groups and PEG contents to optimize for high protein expression after local delivery to the respiratory tract.

In the present work, we created an optimized PACE-mRNA polyplex which achieves high protein expression in the lung— primarily in epithelial cells and antigen presenting cells— without inducing deleterious inflammatory responses. To demonstrate the translational potential of our delivery vehicle, we created an inhalable spike (S) protein mRNA vaccine for SARS-CoV-2. Our vaccine induced *de novo* immunity to SARS-CoV-2 through both systemic and local induction of antibodies. We demonstrated effective draining lymph node germinal center activation, resulting in expansion of S specific memory B cells and antibody secreting cells. Inhaled vaccination induced circulating antigen specific $CD8^+$ T cells and lung resident S specific tissue memory $CD8^+$ T cells. Finally, intranasal PACE-mRNA vaccination protected K18-hACE2 mice from lethal viral challenge. This work represents the first report of an inhaled nonviral, mRNA-based vaccine capable of eliciting *de novo* immunity against SARS-CoV-2 without the need for intramuscular priming.

Results

Characterization of PACE-mRNA polyplexes

We optimized PACE polyplexes for mRNA delivery to the lung by screening novel blends that combine the benefits of PEG stabilization and end group mediated enhanced endosomal escape. We identified 10 promising end group chemistries and synthesized PACE polymers by enzymatic copolymerization of 15-pentadecanolide (PDL), N-methyl diethanolamine (MDEA), and sebacic acid (SA) followed by carbodiimidazole (CDI)-mediated conjugation of amine containing end groups (Fig. 1A, S1-4) (16). A PACE block co-polymer (PACE-PEG) was synthesized by adding a 5 kDa methoxy-ended PEG (mPEG) to the reaction mixture, in a modified literature protocol (15, 18) (table S1).

We administered end group modified PACE-mRNA to human alveolar epithelial cells (A549) and identified PACE with end group 14 (E14) as a promising candidate for delivery (fig. S5). Next, we examined the effect of PACE-PEG content on polyplex characteristics by blending PACE-E14 and PACE-PEG at different ratios. PACE-PEG reduced the size and surface charge of PACE-mRNA polyplexes (Fig. 1B-C), which is consistent with previous reports that PEGylation of cationic polymers can neutralize surface potential (19-21). mRNA loading efficiency was measured using a fluorescent nucleic acid stain (Quant-iT RiboGreen). Although non-PEGylated polyplexes efficiently loaded mRNA (95% loading), the addition of PACE-PEG improved loading efficiency to around 99% (Fig. 1D), suggesting that incorporating PEG can improve the polyplex formulation process.

To provide greater insight into how PEG content affects polyplex structure, we calculated the PEG density and conformation on the surface of PACE-mRNA polyplexes with 1%, 10%, or 25% PACE-PEG by first determining the polyplex molar mass through static light scattering (SLS) measurements (22). We calculated the PEG density on the surface of polyplexes (table S2). Polyplexes with PACE-PEG content of 1-10% (by weight) possessed a surface PEG density in which PEG chains are in a mushroom conformation, whereas 25% PACE-PEG content produces a surface PEG density corresponding to a brush conformation (Fig. 1E).

To compare the mRNA uptake and transfection efficiency of PACE-mRNA polyplexes *in vitro*, we treated A549 cells with polyplexes loaded with Cy5-labeled EGFP mRNA or unlabeled EGFP mRNA using a range of PACE-PEG contents, and we measured the fluorescent signal by microscopy and flow cytometry. Fluorescence microscopy demonstrated that PACE-mRNA without PACE-PEG transfected cells at a comparable rate to a commercial transfection reagent, Lipofectamine MessengerMax (LipoMM). However, we observed a noticeable decrease in EGFP expression at 0.1% and 1% PACE-PEG while the Cy5-labeled mRNA signal remained consistent (Fig. 1F). By flow cytometry, we observed that although polyplex uptake (measured by Cy5-mRNA signal) decreased with the addition of PACE-PEG, the overall uptake was still high; even at 10% PACE-PEG concentration, 99.7% of cells were positive for Cy5 (Fig. 1G). By contrast, the average transfection efficiency (measured by EGFP signal) decreased from 85% to 15% with increasing amounts of PACE-PEG (Fig. 1H). Overall, the incorporation of PACE-PEG caused a decrease in mRNA transfection efficiency that outpaced the drop in mRNA uptake (fig. S6). These results suggest that—while PEGylation inhibits the uptake of PACE polyplexes to some degree—lower uptake doesn't fully explain the inhibitory effect of PEG on mRNA transfection *in vitro*. Based on our prior work demonstrating that mRNA transfection efficiency correlates more strongly with endosomal escape than cellular uptake (16), we hypothesize that PEGylation influences the extent of endosomal escape. In support of this, we noted a decrease in cytoplasmic Cy5-mRNA signal as the extent of PEGylation was increased (Fig. 1F).

The biocompatibility of PACE-mRNA polyplexes with 0%, 10%, and 25% PACE-PEG was compared to LipoMM using the neutral red viability assay. A549 cells were treated with a range of mRNA concentrations, delivered with a consistent ratio of polymer or LipoMM. At higher concentrations, the PACE-mRNA polyplexes were significantly less toxic than LipoMM. There was no significant difference

in viability between the polyplexes based on PEG content (Fig. 1I). These results demonstrate the superiority of PACE-mRNA polyplexes compared to LipoMM in achieving comparably high mRNA transfection efficiency with reduced cytotoxicity *in vitro*.

A primary motivation for encapsulating mRNA into a delivery vehicle is to protect the delicate nucleic acid from abundant degradative enzymes in the lung mucosa. To demonstrate the ability of PACE to protect cargo from RNase activity, we co-incubated PACE-EGFP mRNA polyplexes with RNase before treating HEK293 cells. RNase pretreatment had no significant effect on transfection efficiency as measured by flow cytometry analysis of the EGFP signal (Fig. 1J). PACE preserved the mRNA integrity for delivery to cells, whereas naked mRNA was completely degraded after incubation with RNase under identical conditions (Fig. 1K).

In vivo optimization of PACE-mRNA polyplexes

Prior research has established that traditional cell culture methods are not predictive of transfection *in vivo* for both viral and non-viral delivery systems (5, 17, 23-25). PEGylation of NPs presents additional advantages with administration to mucosal surfaces, as PEGylation is well known to facilitate transport through mucus (26), which is not present in most cell cultures. Therefore, despite the reduced transfection efficiency of PEGylated polyplexes observed *in vitro*, we performed an *in vivo* screen with PACE-PEG content ranging from 0% (no PACE-PEG) to 100% (no PACE-E14). We delivered 5 μg of firefly luciferase (FLuc) mRNA to mice by intratracheal instillation (IT) to assess pulmonary transfection efficiency via a readout of luminescence. At 24 hours, non-PEGylated polyplexes and polyplexes containing up to 50% PACE-PEG had a strong luminescent signal that was 1,000x – 10,000x higher than untreated animals (Fig. 2A). Low amounts of PACE-PEG incorporation (1%, 10%, 25%) improved transfection efficiency compared to non-PEGylated polyplexes, and we observed the highest luminescence with 10% PACE-PEG. With higher levels of PACE-PEG (50%, 100%), there was a significant decrease in luciferase expression, and polyplexes made entirely with PACE-PEG (100%) yielded no luciferase signal. All PACE-mRNA polyplexes containing PACE-E14 content outperformed a commercially available transfection agent, jetRNA. We confirmed these results by *In Vivo* Imaging System (IVIS) imaging, where we observed the highest luminescent signal using 10% PACE-PEG polyplexes (Fig. 2B). We also tracked the luminescent signal after a single delivery over time to see if PEGylation altered the kinetics of mRNA delivery (fig. S7). Luciferase expression was highest at 6 and 24 hours, which is consistent with previous reports of mRNA expression in the lung (11, 27). At 6 and 24 hours, significantly higher luminescence was observed in the group treated with 10% PACE-PEG polyplexes compared to non-PEGylated polyplexes, but at later time points, there was no significant difference between experimental groups. These results demonstrate that low levels of vehicle PEGylation can improve delivery and translation of mRNA, which is consistent with our previous report of mRNA delivery with PACE polyplexes that were not end group-modified (17); however, here we report significantly higher transfection levels—over 100-fold higher by luminescence—demonstrating the significant benefit of using end group-modified (E14) PACE.

Next, we performed IVIS imaging of explanted organs (lungs, spleen, liver, kidneys, and heart), which confirmed that luciferase expression was entirely localized in the lungs, with no observable luminescence coming from other organs (Fig. 2C). High luminescent signal was achieved in both left and right sided lobes of the lung. Using Cy5-labeled mRNA to assess the distribution of IT delivered PACE-mRNA polyplexes (E14 with 10% PACE-PEG) within the pulmonary architecture, we found PACE-mRNA throughout the large airways and into the alveolar regions of the lung parenchyma (Fig. 2D).

While we had found that E14 modified PACE led to optimal *in vitro* epithelial cell transfection efficiency, we wondered if this would hold *in vivo*. To test the *in vivo* efficacy of NPs formed from different end group-modified versions of PACE, we performed an additional screen with all 10 end group-modified PACE polymers (Fig. 1A) and a fixed PACE-PEG content of 10% by weight (Fig. 2E). No measurable luminescent signal was observed following administration of 5 μg of naked mRNA in buffer or with polyplexes produced using the base polymer that did not have a conjugated end group. All end group-modified PACE-mRNA polyplexes achieved significant mRNA expression above control except for E32. We found that E14 remained the top performing end group for transfection in the lung, consistent with our preliminary cell culture-based screen. However, several other end groups also achieved high protein expression. E27 was identified as a second promising end group for PACE-mRNA polyplexes. We further quantified the amount of luciferase protein per gram of total protein in samples extracted from homogenized lungs by comparing to a standard curve of luminescence with recombinant firefly luciferase protein. Quantification of the two formulations with highest mRNA transfection (E14 and E27 with 10% PACE-PEG) each contained more than 1000 ng of FLuc per gram protein in the lung (Fig. 2F).

PACE-mRNA polyplexes transfect epithelial cells and antigen presenting cells in the lung

Having identified two end group-modified PACE polymers (E14 and E27) and the optimal PACE-PEG concentration (10%) for achieving high transfection targeted to the lung, we next characterized cell type-specific mRNA expression in the lung using Ai14 tdTomato reporter mice. Ai14 mice have a loxP-flanked STOP cassette upstream of a tdTomato gene, which can be excised by Cre-mediated recombination, enabling tdTomato expression in the cell (Fig. 3A). After IT instillation of 10 μg of Cre mRNA in PACE-mRNA polyplexes (E14 with 10% PACE-PEG), 9.97% (SD 2.32) of all cells in the lung and 28.8% (SD 12.8) of cells in the bronchoalveolar lavage fluid (BALF) expressed tdTomato (Fig. 3B). We further evaluated the lungs to identify endothelial ($CD31^+$), epithelial ($EpCAM^+$), and leukocyte ($CD45^+$) subpopulations (fig. S8). Transfection was predominantly achieved in epithelial cells and leukocytes, with 21.5% (SD 7.32) of lung epithelial cells and 19.6% (SD 3.47) of lung leukocytes expressing tdTomato. Endothelial cells were not significantly transfected (Fig. 3C). Of the leukocyte cells, we further evaluated markers for antigen presenting cells (APCs) in lung tissue. We found that 59.6% (SD 9.43) of $CD11c^+CD11b^+$ cells and 1.04% (SD 0.28) of $CD11c^+CD11b^-$ cells expressed tdTomato. Fluorescence microscopy of lung sections demonstrated that expression of tdTomato could be found primarily in cells lining the conducting airway and throughout the alveolar regions (Fig. 3E). The localization of fluorescence within the lung architecture is consistent with our flow cytometry finding that transfection occurs primarily in epithelial cells and APCs. We found a similar pattern of expression following delivery of E27 polyplexes. Epithelial cells (16.6% SD 3.83) and antigen presenting $CD11c^+CD11b^+$ cells (58.2% SD 7.34) were most highly transfected. However, total lung cell transfection was slightly reduced (7.37% SD 2.69) (fig. S9).

The *in vivo* biocompatibility of PACE-E14 formulations (with 10% PACE-PEG) was compared to buffer-only treated lungs after 48 hours. Analysis was performed by a pathologist blinded to the treatment group. Histology of treated lungs showed some focal areas with mild neutrophilic infiltrate in the terminal airways only. No evidence of necrosis or other acute airway epithelial change was present (fig. S10).

Intranasal PACE-mRNA vaccination effectively induces antigen specific B and T cell adaptive immune responses in the mediastinal lymph node

Next, we sought to assess whether our top performing PACE-mRNA polyplex (E14 with 10% PACE-PEG) could be applied therapeutically as an inhaled vaccine. We encapsulated mRNA encoding the spike

(S) protein from SARS-CoV-2 into PACE-mRNA polyplexes. We chose a mouse model, K18-hACE2 mice which express human ACE2 (the entry receptor for SARS-CoV-2) from the mouse cytokeratin 18 promoter. K18-hACE2 mice are commonly used in preclinical studies due to their susceptibility to infection and severe pulmonary disease following SARS-CoV-2 viral challenge (28). We used a prime and boost vaccination strategy in which mice received a 10 µg dose of PACE-mRNA delivered intranasally on days 0 and 28. On day 42 (14 days post-boost), we assessed for the development of adaptive immunity against the S protein (Fig. 4A).

To evaluate for effective PACE-mRNA induction of adaptive immune responses, we assessed the mediastinal lymph node (MLN) by flow cytometry for the development of germinal center responses and antigen specific memory and effector B cells and $CD8^+$ T cells, the critical mediators of durable adaptive immunity in the lung (29-31). For identification of S specific T cells, we stained with an MHC class 1 tetramer to a SARS-CoV-2 S protein epitope (VNFNFNGL) and stained B cells with a receptor binding domain (RBD) B cell tetramer. PACE-mRNA vaccination induced a significant population of S specific $CD8^+$ T cells (Fig. 4B). Another T cell subtype important for mounting an adaptive immune response is T follicular helper (T_{FH}) cells. T_{FH} cells promote affinity maturation and class switch recombination in B cells and critically orchestrate the development of neutralizing antibody responses (32). Systemically administered mRNA vaccines elicit T_{FH} and germinal center B cells, which strongly correlates with neutralizing antibody production (33, 34). We found significant induction of T follicular helper (T_{FH}) cells in the MLN (Fig. 4C). Correspondingly, there was significant expansion of S specific B cells ($CD19^+B220^+Tetramer^+$), class switched B cells expressing IgA and IgG ($CD19^+B220^+IgD^-IgM^-$), activated germinal center B cells ($CD19^+B220^+GL7^+$), and antibody secreting cells ($CD138^+$) in the MLN (Fig. 4D-I). These results demonstrated that PACE-mRNA vaccination induces potent antigen specific T and B cell responses in the draining lymph node following mucosal delivery. Further, S specific B cells expressed memory markers demonstrating promise for the efficacy and durability of the adaptive immune response after PACE-mRNA vaccination.

Intranasal PACE-mRNA vaccination confers protective tissue resident and circulating immunity against SARS-CoV-2 viral challenge

Finally, we assessed lung tissue, serum, and BALF for local and systemic antigen specific T cells and antibodies. We used intravenous (IV) labeling of CD45 to differentiate between circulating and tissue resident immune cells. Additionally, 4 weeks after boost delivery (day 56), we challenged naïve and PACE-mRNA vaccinated K18-hACE2 mice with a lethal dose of SARS-CoV-2 (Fig. 5A). Consistent with our findings in the MLN, we found that vaccination induced a significant population of S specific $CD8^+$ T cells in the lung parenchyma (IV^-) (Fig. 5B). S specific $CD8^+$ T cells significantly expressed tissue resident memory (T_{RM}) surface markers, $CD69^+$ and $CD103^+$ (Fig. 5C-D). We also found significant increases in systemic circulating antigen specific $CD8^+$ T cells harvested from the lungs ($IV^+Tetramer^+CD8^+$) (Fig. 5E). These results demonstrate that vaccination elicited both a lung resident and a circulating $CD8^+$ T cell response. Currently available intramuscularly administered vaccines induce circulating but not lung resident S specific T_{RM} responses (29), highlighting the advantage of our mucosal PACE-mRNA delivery strategy.

We assessed serum and BALF for anti-SARS-CoV-2 spike S1 IgG and IgA to determine whether mucosal vaccination induced humoral immunity. We found that both circulating (serum) and mucosal (BALF) IgG antibodies were significantly induced (Fig. 5F-G), but IgA was not significantly induced (fig. S11). Finally, to assess whether the demonstrated adaptive immunity would protect mice from viral infection, we challenged mice with a lethal dose ($6x10^5$ PFU) of SARS-CoV-2. Weight loss and survival

in vaccinated mice were both significantly improved (Fig. 5H-J), demonstrating the protective efficacy of our PACE-mRNA polyplexes.

Discussion

We have demonstrated that PACE polymer formulations can be optimized and applied for local mRNA delivery to the lung. We employed a screening method for optimizing polyplexes, a strategy which has previously been employed for lipopolyplex (25) and LNP (35-37) optimization. LNP optimization often requires screening varying ratios of four component variables, generating large and unwieldy chemical spaces. Our polyplexes required only two components which facilitated screening efficiency. We showed that a relatively simple polyplex design containing 90% end group-modified PACE (PACE-E14) and 10% PACE-PEG complexed with mRNA to form small and stable polyplexes which protect mRNA from enzymatic degradation and achieve high *in vivo* transfection efficiency.

By calculating the PEG surface density, we gained insight into how PEG content affects polyplex structure. The change in conformation from the more compact mushroom to the brush conformation at 25% PACE-PEG corresponded with the drop in transfection efficiency observed *in vivo* with higher PACE-PEG content. These results are consistent with previous studies demonstrating that PEG surface coverage at high densities can interfere with cellular uptake *in vivo* (17, 23). The transition from the mushroom to the brush conformation results in a thicker hydrophilic barrier, thereby decreasing the potential for interaction between the cell membrane and the PACE end group. This data demonstrates that conformational changes that decrease the exposure of cationic surface elements can interfere with transfection.

This work represents the first polyplexes of end group-modified PACE with PACE-PEG polymers and the first investigation of end group-modified PACE-mRNA in the lung. Previous work in both polymer (38, 39) and lipid (40, 41) design has demonstrated that amine containing end groups can increase mRNA expression or particle targeting to the lung. Our screen identified several amine-containing end groups that increase expression in the lung. The top performing end groups in our screen (E14 and E27) were not the same end groups which transfected most efficiently following intravenous administration of unPEGylated PACE-mRNA polyplexes (16), supporting the need for compartment-specific optimization of delivery vehicles.

Our optimized PACE polyplexes facilitated significant mRNA transfection into epithelial cells and antigen presenting cells. Ease of epithelial cell targeting is a primary advantage of inhaled delivery strategies (27). Protein replacement therapy via mRNA delivery to epithelial cells is therapeutically relevant for a host of diseases such as cystic fibrosis (CF) (42), asthma (43), surfactant B protein deficiency (44), and alpha-1-antitrypsin deficiency (45). Our epithelial transfection rate of >20% after a single dose suggests that protein expression will be therapeutically relevant; prior research has shown that for significant disease mitigation only a fraction of lung cells in CF need to express CFTR. For example, 17-28% of cells expressing CFTR in a porcine lung model restored 50% of normal CFTR function, an amount consistent with significant amelioration of symptoms (46). Previous attempts to deliver inhaled mRNA in preclinical models (47, 48) have achieved moderate success in disease treatment, demonstrating both proof of concept for the therapeutic avenue and the need for further innovation. The significant epithelial protein expression and the tolerability of repeated doses of the PACE vehicles described here supports further investigation for protein supplementation applications in the lung.

For effective mucosal vaccination, mRNA targeting to APCs, which process and present antigen to other immune cells, is critical for vaccine efficacy (49). Due to the on-going global SARS-CoV-2 pandemic and high APC transfection with our platform, we chose to test the therapeutic potential of inhaled PACE-mRNA polyplexes as a mucosal vaccine against SARS-CoV-2. The rapid development of mRNA-based vaccines for SARS-CoV-2 was a historic achievement. To date, over 200 million US citizens have been vaccinated with Comirnaty or Spikevax. Not only were they the first vaccines to demonstrate safety and efficacy in reducing viral transmission, hospitalization, and death, but also the first mRNA-based therapeutics to gain FDA approval. Both vaccines target the S protein on the surface of the SARS-CoV-2 virus and deliver their mRNA cargo encapsulated in LNPs. These vaccines have the highest efficacy rates of all the vaccine platforms employed to combat the SARS-CoV-2 pandemic globally (50). Despite the remarkable safety and initial efficacy, declining immunity over time is a major limitation of these and other current vaccine platforms (51). Additionally, the continued emergence of new viral variants of concern (VOC) has further reduced vaccine efficacy (52-55). These limitations have spurred interest in new vaccination technologies that can combat the ongoing challenges posed by the SARS-CoV-2 pandemic.

Current mRNA vaccination strategies are focused on eliciting systemic immunity, primarily through the induction of IgG antibodies in serum and circulating antigen specific T cells (56, 57). However, growing evidence supports the superior effectiveness of vaccines that are delivered directly to the respiratory tract to combat respiratory viruses (58). The respiratory tract is the site of invasion and primary site of replication and disease manifestation for SARS-CoV-2 and its variants. Several studies investigating viral vector and protein-based vaccines have demonstrated that superior mucosal immunity can be achieved through direct antigen presentation across the mucosal surface of the lung (59-62). Mucosal vaccination strategies have been shown to improve upon systemic vaccination through the induction of tissue resident memory T and B cells, which can rapidly respond to viral invasion into the respiratory tract (31, 63). Additionally, mucosal vaccination can induce higher levels of antibodies in the respiratory mucosa (59). The induction of robust mucosal cellular and humoral immunity can more rapidly neutralize viruses upon entry into the respiratory tract, thereby preventing both infection and transmission (60).

Our PACE-mRNA vaccine induced both circulating and lung resident S specific $CD8^+$ T cells, S specific memory B cells, and anti-S1 IgG in both serum and airways. The efficacy of PACE-mRNA as a mucosal vaccination strategy supports further investigation for respiratory viruses. Despite the impressive performance of approved mRNA-based vaccines and the potential to enhance protective immunity through mucosal delivery, as of the writing of this manuscript no mRNA-based vaccines have been reported to prevent SARS-CoV-2 infection following respiratory mucosal administration. This work is the first inhaled non-viral vector mRNA vaccine to demonstrate tolerability for repeated dosing and *de novo* induction of protective immunity against SARS-CoV-2.

Conclusions

In summary, PACE-mRNA polyplexes can be formulated with blends of an end group-modified PACE and PACE-PEG to form small, consistent, and stable polyplexes. PACE polyplexes demonstrate favorable biocompatibility and protect mRNA from degradative enzymes. PEG content can improve polyplex characteristics (smaller size, more neutral surface potential, high mRNA loading) however dense PEG shells can interfere with transfection efficiency. Therefore, PEG content was optimized for lung specific delivery. Inhaled PACE-mRNA administration achieved high protein expression and effective lung targeting. Transfection occurred primarily in lung epithelial cells and APCs, two cell types which are

highly relevant targets for a host of pulmonary diseases. Mucosal vaccination with PACE-mRNA induced systemic and lung resident adaptive immunity and protected mice from a lethal viral challenge.

References

1. Polack FP, Thomas SJ, Kitchin N, Absalon J, Gurtman A, Lockhart S, et al. Safety and Efficacy of the BNT162b2 mRNA Covid-19 Vaccine. N Engl J Med. 2020;383(27):2603-15.
2. Baden LR, El Sahly HM, Essink B, Kotloff K, Frey S, Novak R, et al. Efficacy and Safety of the mRNA-1273 SARS-CoV-2 Vaccine. N Engl J Med. 2021;384(5):403-16.
3. Pardi N, Hogan MJ, Porter FW, Weissman D. mRNA vaccines - a new era in vaccinology. Nat Rev Drug Discov. 2018;17(4):261-79.
4. Kowalski PS, Rudra A, Miao L, Anderson DG. Delivering the Messenger: Advances in Technologies for Therapeutic mRNA Delivery. Mol Ther. 2019;27(4):710-28.
5. Piotrowski-Daspit AS, Kauffman AC, Bracaglia LG, Saltzman WM. Polymeric vehicles for nucleic acid delivery. Adv Drug Deliv Rev. 2020;156:119-32.
6. Chow MYT, Chang RYK, Chan HK. Inhalation delivery technology for genome-editing of respiratory diseases. Adv Drug Deliv Rev. 2021;168:217-28.
7. Chow MYT, Qiu Y, Lam JKW. Inhaled RNA Therapy: From Promise to Reality. Trends Pharmacol Sci. 2020;41(10):715-29.
8. Sahu I, Haque A, Weidensee B, Weinmann P, Kormann MSD. Recent Developments in mRNA-Based Protein Supplementation Therapy to Target Lung Diseases. Mol Ther. 2019;27(4):803-23.
9. Tang J, Cai L, Xu C, Sun S, Liu Y, Rosenecker J, et al. Nanotechnologies in Delivery of DNA and mRNA Vaccines to the Nasal and Pulmonary Mucosa. Nanomaterials (Basel). 2022;12(2).
10. Ndeupen S, Qin Z, Jacobsen S, Bouteau A, Estanbouli H, Igyártó BZ. The mRNA-LNP platform's lipid nanoparticle component used in preclinical vaccine studies is highly inflammatory. iScience. 2021;24(12):103479.
11. Pardi N, Tuyishime S, Muramatsu H, Kariko K, Mui BL, Tam YK, et al. Expression kinetics of nucleoside-modified mRNA delivered in lipid nanoparticles to mice by various routes. J Control Release. 2015;217:345-51.
12. Translate Bio Announces Results from Second Interim Data Analysis from Ongoing Phase 1/2 Clinical Trial of MRT5005 in Patients with Cystic Fibrosis (CF) [press release]. Translate Bio, March 17, 2021 2021.
13. Mutsch M, Zhou W, Rhodes P, Bopp M, Chen RT, Linder T, et al. Use of the inactivated intranasal influenza vaccine and the risk of Bell's palsy in Switzerland. N Engl J Med. 2004;350(9):896-903.
14. Zhou J, Liu J, Cheng CJ, Patel TR, Weller CE, Piepmeier JM, et al. Biodegradable poly(amine-co-ester) terpolymers for targeted gene delivery. Nat Mater. 2011;11(1):82-90.
15. Kauffman AC, Piotrowski-Daspit AS, Nakazawa KH, Jiang Y, Datye A, Saltzman WM. Tunability of Biodegradable Poly(amine- co-ester) Polymers for Customized Nucleic Acid Delivery and Other Biomedical Applications. Biomacromolecules. 2018;19(9):3861-73.
16. Jiang Y, Lu Q, Wang Y, Xu E, Ho A, Singh P, et al. Quantitating Endosomal Escape of a Library of Polymers for mRNA Delivery. Nano Lett. 2020;20(2):1117-23.
17. Grun MK, Suberi A, Shin K, Lee T, Gomerdinger V, Moscato ZM, et al. PEGylation of poly(amine-co-ester) polyplexes for tunable gene delivery. Biomaterials. 2021;272:120780.
18. Zhang X, Liu B, Yang Z, Zhang C, Li H, Luo X, et al. Micelles of enzymatically synthesized PEG-poly(amine-co-ester) block copolymers as pH-responsive nanocarriers for docetaxel delivery. Colloids and Surfaces B: Biointerfaces. 2014;115:349-58.
19. Ogris M, Brunner S, Schüller S, Kircheis R, Wagner E. PEGylated DNA/transferrin-PEI complexes: reduced interaction with blood components, extended circulation in blood and potential for systemic gene delivery. Gene Ther. 1999;6(4):595-605.

20. Oupicky D, Ogris M, Howard KA, Dash PR, Ulbrich K, Seymour LW. Importance of lateral and steric stabilization of polyelectrolyte gene delivery vectors for extended systemic circulation. Mol Ther. 2002;5(4):463-72.
21. Sung SJ, Min SH, Cho KY, Lee S, Min YJ, Yeom YI, et al. Effect of polyethylene glycol on gene delivery of polyethylenimine. Biol Pharm Bull. 2003;26(4):492-500.
22. Cao ZT, Gan LQ, Jiang W, Wang JL, Zhang HB, Zhang Y, et al. Protein Binding Affinity of Polymeric Nanoparticles as a Direct Indicator of Their Pharmacokinetics. ACS Nano. 2020;14(3):3563-75.
23. Osman G, Rodriguez J, Chan SY, Chisholm J, Duncan G, Kim N, et al. PEGylated enhanced cell penetrating peptide nanoparticles for lung gene therapy. J Control Release. 2018;285:35-45.
24. Nelson CE, Kintzing JR, Hanna A, Shannon JM, Gupta MK, Duvall CL. Balancing cationic and hydrophobic content of PEGylated siRNA polyplexes enhances endosome escape, stability, blood circulation time, and bioactivity in vivo. ACS Nano. 2013;7(10):8870-80.
25. Kaczmarek JC, Kauffman KJ, Fenton OS, Sadtler K, Patel AK, Heartlein MW, et al. Optimization of a Degradable Polymer-Lipid Nanoparticle for Potent Systemic Delivery of mRNA to the Lung Endothelium and Immune Cells. Nano Lett. 2018;18(10):6449-54.
26. Cu Y, Saltzman WM. Controlled surface modification with poly(ethylene)glycol enhances diffusion of PLGA nanoparticles in human cervical mucus. Mol Pharm. 2009;6(1):173-81.
27. Patel AK, Kaczmarek JC, Bose S, Kauffman KJ, Mir F, Heartlein MW, et al. Inhaled Nanoformulated mRNA Polyplexes for Protein Production in Lung Epithelium. Adv Mater. 2019;31(8):e1805116.
28. Winkler ES, Bailey AL, Kafai NM, Nair S, McCune BT, Yu J, et al. SARS-CoV-2 infection of human ACE2-transgenic mice causes severe lung inflammation and impaired function. Nature Immunology. 2020;21(11):1327-35.
29. Israelow B, Mao T, Klein J, Song E, Menasche B, Omer SB, et al. Adaptive immune determinants of viral clearance and protection in mouse models of SARS-CoV-2. Sci Immunol. 2021;6(64):eabl4509.
30. Knight FC, Wilson JT. Engineering Vaccines for Tissue-Resident Memory T Cells. Adv Ther (Weinh). 2021;4(4).
31. Allie SR, Bradley JE, Mudunuru U, Schultz MD, Graf BA, Lund FE, et al. The establishment of resident memory B cells in the lung requires local antigen encounter. Nat Immunol. 2019;20(1):97-108.
32. Krishnaswamy JK, Alsén S, Yrlid U, Eisenbarth SC, Williams A. Determination of T Follicular Helper Cell Fate by Dendritic Cells. Frontiers in Immunology. 2018;9.
33. Lederer K, Castaño D, Gómez Atria D, Oguin TH, 3rd, Wang S, Manzoni TB, et al. SARS-CoV-2 mRNA Vaccines Foster Potent Antigen-Specific Germinal Center Responses Associated with Neutralizing Antibody Generation. Immunity. 2020;53(6):1281-95.e5.
34. Turner JS, O'Halloran JA, Kalaidina E, Kim W, Schmitz AJ, Zhou JQ, et al. SARS-CoV-2 mRNA vaccines induce persistent human germinal centre responses. Nature. 2021;596(7870):109-13.
35. Lokugamage MP, Vanover D, Beyersdorf J, Hatit MZC, Rotolo L, Echeverri ES, et al. Optimization of lipid nanoparticles for the delivery of nebulized therapeutic mRNA to the lungs. Nat Biomed Eng. 2021;5(9):1059-68.
36. Kauffman KJ, Dorkin JR, Yang JH, Heartlein MW, DeRosa F, Mir FF, et al. Optimization of Lipid Nanoparticle Formulations for mRNA Delivery in Vivo with Fractional Factorial and Definitive Screening Designs. Nano Lett. 2015;15(11):7300-6.
37. Zhang H, Leal J, Soto MR, Smyth HDC, Ghosh D. Aerosolizable Lipid Nanoparticles for Pulmonary Delivery of mRNA through Design of Experiments. Pharmaceutics. 2020;12(11).
38. Jarzębińska A, Pasewald T, Lambrecht J, Mykhaylyk O, Kümmerling L, Beck P, et al. A Single Methylene Group in Oligoalkylamine-Based Cationic Polymers and Lipids Promotes Enhanced mRNA Delivery. Angew Chem Int Ed Engl. 2016;55(33):9591-5.

39. Kowalski PS, Capasso Palmiero U, Huang Y, Rudra A, Langer R, Anderson DG. Ionizable Amino-Polyesters Synthesized via Ring Opening Polymerization of Tertiary Amino-Alcohols for Tissue Selective mRNA Delivery. Adv Mater. 2018:e1801151.
40. Cheng Q, Wei T, Farbiak L, Johnson LT, Dilliard SA, Siegwart DJ. Selective organ targeting (SORT) nanoparticles for tissue-specific mRNA delivery and CRISPR-Cas gene editing. Nat Nanotechnol. 2020;15(4):313-20.
41. Qiu M, Tang Y, Chen J, Muriph R, Ye Z, Huang C, et al. Lung-selective mRNA delivery of synthetic lipid nanoparticles for the treatment of pulmonary lymphangioleiomyomatosis. Proc Natl Acad Sci U S A. 2022;119(8).
42. Da Silva Sanchez A, Paunovska K, Cristian A, Dahlman JE. Treating Cystic Fibrosis with mRNA and CRISPR. Hum Gene Ther. 2020;31(17-18):940-55.
43. Zeyer F, Mothes B, Will C, Carevic M, Rottenberger J, Nürnberg B, et al. mRNA-Mediated Gene Supplementation of Toll-Like Receptors as Treatment Strategy for Asthma In Vivo. PLoS One. 2016;11(4):e0154001.
44. Kormann MS, Hasenpusch G, Aneja MK, Nica G, Flemmer AW, Herber-Jonat S, et al. Expression of therapeutic proteins after delivery of chemically modified mRNA in mice. Nat Biotechnol. 2011;29(2):154-7.
45. Guan S, Darmstädter M, Xu C, Rosenecker J. In Vitro Investigations on Optimizing and Nebulization of IVT-mRNA Formulations for Potential Pulmonary-Based Alpha-1-Antitrypsin Deficiency Treatment. Pharmaceutics. 2021;13(8).
46. Potash AE, Wallen TJ, Karp PH, Ernst S, Moninger TO, Gansemer ND, et al. Adenoviral gene transfer corrects the ion transport defect in the sinus epithelia of a porcine CF model. Mol Ther. 2013;21(5):947-53.
47. Haque A, Dewerth A, Antony JS, Riethmüller J, Schweizer GR, Weinmann P, et al. Chemically modified hCFTR mRNAs recuperate lung function in a mouse model of cystic fibrosis. Sci Rep. 2018;8(1):16776.
48. Robinson E, MacDonald KD, Slaughter K, McKinney M, Patel S, Sun C, et al. Lipid Nanoparticle-Delivered Chemically Modified mRNA Restores Chloride Secretion in Cystic Fibrosis. Mol Ther. 2018;26(8):2034-46.
49. Cohn L, Delamarre L. Dendritic Cell-Targeted Vaccines. Frontiers in Immunology. 2014;5.
50. Self WH, Tenforde MW, Rhoads JP, al e. Comparative Effectiveness of Moderna, Pfizer-BioNTech, and Janssen (Johnson & Johnson) Vaccines in Preventing COVID-19 Hospitalizations Among Adults Without Immunocompromising Conditions — United States, March–August 2021. MMWR Morb Mortal Wkly Rep 2021. 2021(70):1337–43.
51. Ferdinands JM, Rao S, Dixon BE, al. e. Waning 2-Dose and 3-Dose Effectiveness of mRNA Vaccines Against COVID-19–Associated Emergency Department and Urgent Care Encounters and Hospitalizations Among Adults During Periods of Delta and Omicron Variant Predominance — VISION Network, 10 States, August 2021–January 2022. MMWR Morb Mortal Wkly Rep. 2022(71):255–63.
52. Lucas C, Vogels CBF, Yildirim I, Rothman JE, Lu P, Monteiro V, et al. Impact of circulating SARS-CoV-2 variants on mRNA vaccine-induced immunity. Nature. 2021;600(7889):523-9.
53. Lopez Bernal J, Andrews N, Gower C, Gallagher E, Simmons R, Thelwall S, et al. Effectiveness of Covid-19 Vaccines against the B.1.617.2 (Delta) Variant. N Engl J Med. 2021;385(7):585-94.
54. Bruxvoort KJ, Sy LS, Qian L, Ackerson BK, Luo Y, Lee GS, et al. Effectiveness of mRNA-1273 against delta, mu, and other emerging variants of SARS-CoV-2: test negative case-control study. Bmj. 2021;375:e068848.
55. Collie S, Champion J, Moultrie H, Bekker LG, Gray G. Effectiveness of BNT162b2 Vaccine against Omicron Variant in South Africa. N Engl J Med. 2022;386(5):494-6.

56. Corbett KS, Edwards DK, Leist SR, Abiona OM, Boyoglu-Barnum S, Gillespie RA, et al. SARS-CoV-2 mRNA vaccine design enabled by prototype pathogen preparedness. Nature. 2020;586(7830):567-71.
57. Vogel AB, Kanevsky I, Che Y, Swanson KA, Muik A, Vormehr M, et al. BNT162b vaccines protect rhesus macaques from SARS-CoV-2. Nature. 2021;592(7853):283-9.
58. Heida R, Hinrichs WL, Frijlink HW. Inhaled vaccine delivery in the combat against respiratory viruses: a 2021 overview of recent developments and implications for COVID-19. Expert Rev Vaccines. 2021:1-18.
59. Mao T, Israelow B, Suberi A, Zhou L, Reschke M, Peña-Hernández MA, et al. Unadjuvanted intranasal spike vaccine booster elicits robust protective mucosal immunity against sarbecoviruses. bioRxiv. 2022.
60. An D, Li K, Rowe DK, Diaz MCH, Griffin EF, Beavis AC, et al. Protection of K18-hACE2 mice and ferrets against SARS-CoV-2 challenge by a single-dose mucosal immunization with a parainfluenza virus 5-based COVID-19 vaccine. Sci Adv. 2021;7(27).
61. Afkhami S, D'Agostino MR, Zhang A, Stacey HD, Marzok A, Kang A, et al. Respiratory mucosal delivery of next-generation COVID-19 vaccine provides robust protection against both ancestral and variant strains of SARS-CoV-2. Cell. 2022.
62. Hassan AO, Kafai NM, Dmitriev IP, Fox JM, Smith BK, Harvey IB, et al. A Single-Dose Intranasal ChAd Vaccine Protects Upper and Lower Respiratory Tracts against SARS-CoV-2. Cell. 2020;183(1):169-84.e13.
63. Li AV, Moon JJ, Abraham W, Suh H, Elkhader J, Seidman MA, et al. Generation of effector memory T cell-based mucosal and systemic immunity with pulmonary nanoparticle vaccination. Sci Transl Med. 2013;5(204):204ra130.
64. Repetto G, del Peso A, Zurita JL. Neutral red uptake assay for the estimation of cell viability/cytotoxicity. Nat Protoc. 2008;3(7):1125-31.
65. Israelow B, Song E, Mao T, Lu P, Meir A, Liu F, et al. Mouse model of SARS-CoV-2 reveals inflammatory role of type I interferon signaling. J Exp Med. 2020;217(12).
66. Mao T, Israelow B, Lucas C, Vogels CBF, Gomez-Calvo ML, Fedorova O, et al. A stem-loop RNA RIG-I agonist protects against acute and chronic SARS-CoV-2 infection in mice. J Exp Med. 2022;219(1).

Acknowledgements
This work was supported by NIH grants UG3 HL147352 and R01 AI157488, the Fast Grant from Emergent Ventures at the Mercatus Center, and HHMI funding dedicated to collaborative research projects on SARS-CoV-2 and the disease it causes, COVID-19. A.S. is supported by the NIGMS T32GM136651. A.I. is an Investigator of the Howard Hughes Medical Institute. B.I. is supported by NIAID T32AI007517 and K08AI163493. T.M. is supported by NIAID T32AI007019. A.S.P. is supported by a K99/R00 Pathway to Independence award from the NIH (K99 HL151806) and a Postdoc-to-Faculty Transition Award from the Cystic Fibrosis Foundation (CFF; PIOTRO21F5).

Author contributions
Conceptualization: AS, AI, WMS

Methodology: AS, MKG, HS, TM, BI, MR, JG, TL

Investigation: AS, MKG, HS, TM, BI, MR, JG, LA, TL, KS, ASP, RH

Visualization: AS, MKG, TM, BI

Funding acquisition: AI, WMS

Project administration: AI, HS, WMS

Supervision: AI, HS, WMS

Writing – original draft: AS, MKG

Writing – review & editing: AS, MKG, HS, TM, BI, MR, JG, LA, TL, KS, ASP, RH, AI, WMS

Competing Interests Statement
A.S.P., A.I., and W.M.S are cofounders of Xanadu Bio, and B.I. and T.M. serve as consultants for Xanadu Bio. A.I., B.I., and T.M. are listed as inventors on patent applications relating to intranasal spike-based SARS-CoV-2 vaccines filed by Yale University. A.I., W.M.S., B.I., T.M, A.S., M.H., A.S.P., and H.S. are listed as inventors on patent applications relating to intranasal PACE nanoparticle delivery-based vaccines filed by Yale University. A.S., M.K.G., and W.M.S are listed as inventors on patent applications relating to PACE-mRNA delivery to the lung filed by Yale University.

Corresponding Authors: Correspondence and requests for data or materials should be addressed to H.S. or W.M.S

Supplementary Materials
Materials and Methods
Figs. S1 to S12
Table S1 to S2

Fig 1. Characterization of PACE-mRNA polyplexes and *in vitro* activity. (**A**) Schematic of end group-modified and PEGylated PACE polymer composition with chemical structures of base monomers and end groups (**B**) Size and PDI; (**C**) zeta potential; (**D**) mRNA loading; and (**E**) PEG conformation on the surface of PACE-E14 polyplexes with varying PACE-PEG content. R_f represents PEG Flory radius and D the distance between PEG chains. Asterisks indicate statistical difference from non-PEGylated polyplexes. (**F**) Representative mRNA uptake and transfection efficiency of Cy5-conjugated EGFP mRNA delivered with PACE-PEG blended polyplexes (scale bar, 75 μm). (**G**) Uptake of Cy5-conjugated mRNA and (**H**) transfection efficiency of EGFP mRNA in A549 cells with PEGylated PACE-E14. (**I**) *In vitro* cytotoxicity of PEGylated PACE-E14 polyplexes compared to Lipofectamine MessengerMAX. Asterisks indicate differences between all PACE polyplexes and Lipofectamine. (**J-K**) Transfection efficiency of EGFP mRNA PACE-E14 polyplexes in HEK293T cells with or without coincubation of RNase and a gel run with either naked mRNA or mRNA and RNase showing degradation of mRNA by the enzyme. * $p \leq 0.05$, ** $p \leq 0.01$, *** $p \leq 0.001$, **** $p \leq 0.0001$. Data are pooled from two independent experiments.

Fig 2. IT mRNA delivery with PACE-mRNA polyplexes provides significant protein expression and mRNA distribution throughout the airways and parenchyma. (**A**) Luciferase protein expression in lung tissue after delivery of FLuc mRNA with PEGylated PACE-E14 and *in vivo*-jetRNA. Sample means of log-transformed values were compared by Tukey's multiple comparison test. (**B**) Representative luciferase expression by IVIS 24 hours after IT delivery of PACE-E14 10% PACE-PEG FLuc mRNA polyplexes in animals and (**C**) in explanted organs. (**D**) Distribution of Cy5-conjugated mRNA in the lung 30 minutes after delivery with PACE-E14 polyplexes (scale bar, 150 μm). (**E**) Luciferase protein expression in lung tissue after delivery of FLuc mRNA with polyplexes of various end group modified and 10% PACE-PEG content, untreated control, naked mRNA control, and base polymer with no end group control. (**F**) Quantification of luciferase protein extracted from lungs 24 hours after treatment with either E14 or E27 polyplexes with 10% PACE-PEG. * $p \leq 0.05$, ** $p \leq 0.01$, *** $p \leq 0.001$, **** $p \leq 0.0001$. Data are pooled from two independent experiments.

Fig 3. mRNA expression after IT PACE-mRNA delivery occurs in epithelial cells and APCs. (**A**) Schematic of Cre mediated recombination in Ai14 mice resulting in expression of tdTomato protein in transfected cells. Percent of (**B**) all live cells in the lung and BALF, (**C**) endothelial, epithelial, or leukocyte cells in the lung and (**D**) APCs in the lung that express tdTomato 24 hours after administration of PACE-E14 polyplexes (10% PACE-PEG) loaded with Cre mRNA. Statistical significance was calculated by multiple unpaired t-test with holm-sidak method. (**E**) Representative images of control (untreated) and PACE-E14 polyplex (10% PACE-PEG) treated lungs from Ai14 mice by fluorescence microscopy (scale bar, 100 μm, DAPI in blue, tdTomato in red). * $p \leq 0.05$, ** $p \leq 0.01$, *** $p \leq 0.001$, **** $p \leq 0.0001$. Data are pooled from two independent experiments.

Fig 4. IN PACE-mRNA vaccination induces antigen specific T and B cell responses in the draining lymph node. (**A**) Schematic of PACE-mRNA vaccination in K18-hACE2 mice. Mice were primed (day 0) and boosted (day 28) with a 10 μg dose of S protein mRNA encapsulated in PACE-E14 polyplexes with 10% PACE-PEG. MLN were harvested on day 42 for analysis. (**B**) Quantification of extravascular (IV^-) SCV2 spike-specific $Tetramer^+$ CD8 T cells in MLN. (**C**) Quantification of extravascular (IV^-) $CXCR5^+PD1^+$ T_{FH} cells in MLN. (**D-I**) Quantification of various extravascular B cell subsets, including RBD tetramer-binding B cells, class switched B cells, IgA^+ memory B cells, IgG^+ memory B cells, activated germinal center B cells, and antibody secreting cells in MLN. Mean ± s.e.m.; Statistical

significance was calculated by student's t-test. * $p \leq 0.05$, ** $p \leq 0.01$, *** $p \leq 0.001$, **** $p \leq 0.0001$. Data are pooled from two independent experiments.

Fig 5. IN PACE-mRNA vaccination induces protective cellular and humoral immunity. (**A**) Schematic of PACE-mRNA vaccination in K18-hACE2 mice. Mice were primed (day 0) and boosted (day 28) with a 10 μg dose of S protein mRNA encapsulated in PACE-E14 polyplexes with 10% PACE-PEG. Lungs, serum, and BALF were harvested on day 42 for analysis. An additional group of vaccinated animals was challenged with $6x10^5$ PFU of SARS-CoV-2 on day 56 and weight loss and survival were evaluated over two weeks compared to untreated naïve mice. (**B-D**) Quantification of extravascular (IV^-) SCV2 spike-specific $Tetramer^+$ CD8 T cells, $CD69^+CD103^-Tetramer^+$ CD8 T cells, or $CD69^+CD103^+Tetramer^+$ CD8 T cells in the lung. (**E**) Quantification of circulating (IV^+) SCV2 spike-specific $Tetramer^+$ CD8 T cells from lung vasculature. (**F**) Serum and (**G**) BALF measurement of SCV2 spike S1 subunit-specific IgG. Mean ± s.e.m.; Statistical significance was calculated by student's t-test. (**H-I**) Average and (**I**) individual weight measurements after viral challenge in naïve and PACE-mRNA vaccinated mice. (**J**) Survival of naïve and vaccinated mice from 1 to 14 days post infection. Mean ± s.e.m.; Statistical significance was calculated by log-rank Mantel–Cox test. * $p \leq 0.05$, ** $p \leq 0.01$, *** $p \leq 0.001$, **** $p \leq 0.0001$. Data are pooled from two independent experiments.

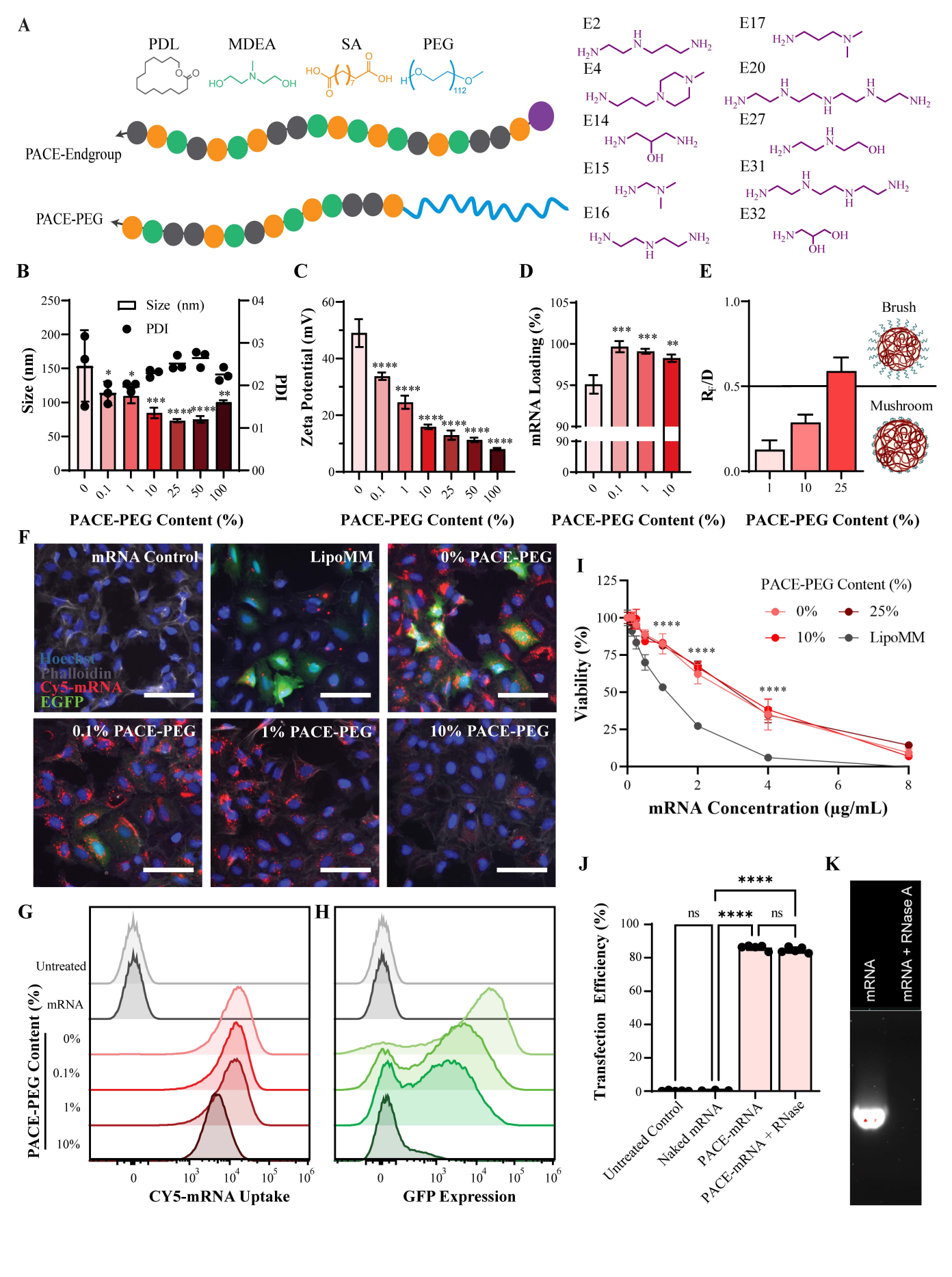
A
PDL
MDEA
SA
PEG
PACE-Endgroup
PACE-PEG
E2
E4
E14
E15
E16
E17
E20
E27
E31
E32
B
Size (nm)
PDI
PACE-PEG Content (%)
C
Zeta Potential (mV)
PACE-PEG Content (%)
D
mRNA Loading (%)
PACE-PEG Content (%)
E
Brush
Mushroom
PACE-PEG Content (%)
F
mRNA Control
LipoMM
0% PACE-PEG
0.1% PACE-PEG
1% PACE-PEG
10% PACE-PEG
Hoechst
Phalloidin
Cy5-mRNA
EGFP
I
PACE-PEG Content (%)
0%
10%
25%
LipoMM
Viability (%)
mRNA Concentration (μg/mL)
G
Untreated
mRNA
0%
0.1%
1%
10%
PACE-PEG Content (%)
CY5-mRNA Uptake
H
GFP Expression
J
Transfection Efficiency (%)
ns
Untreated Control
Naked mRNA
PACE-mRNA
PACE-mRNA + RNase
K
mRNA
mRNA + RNase A

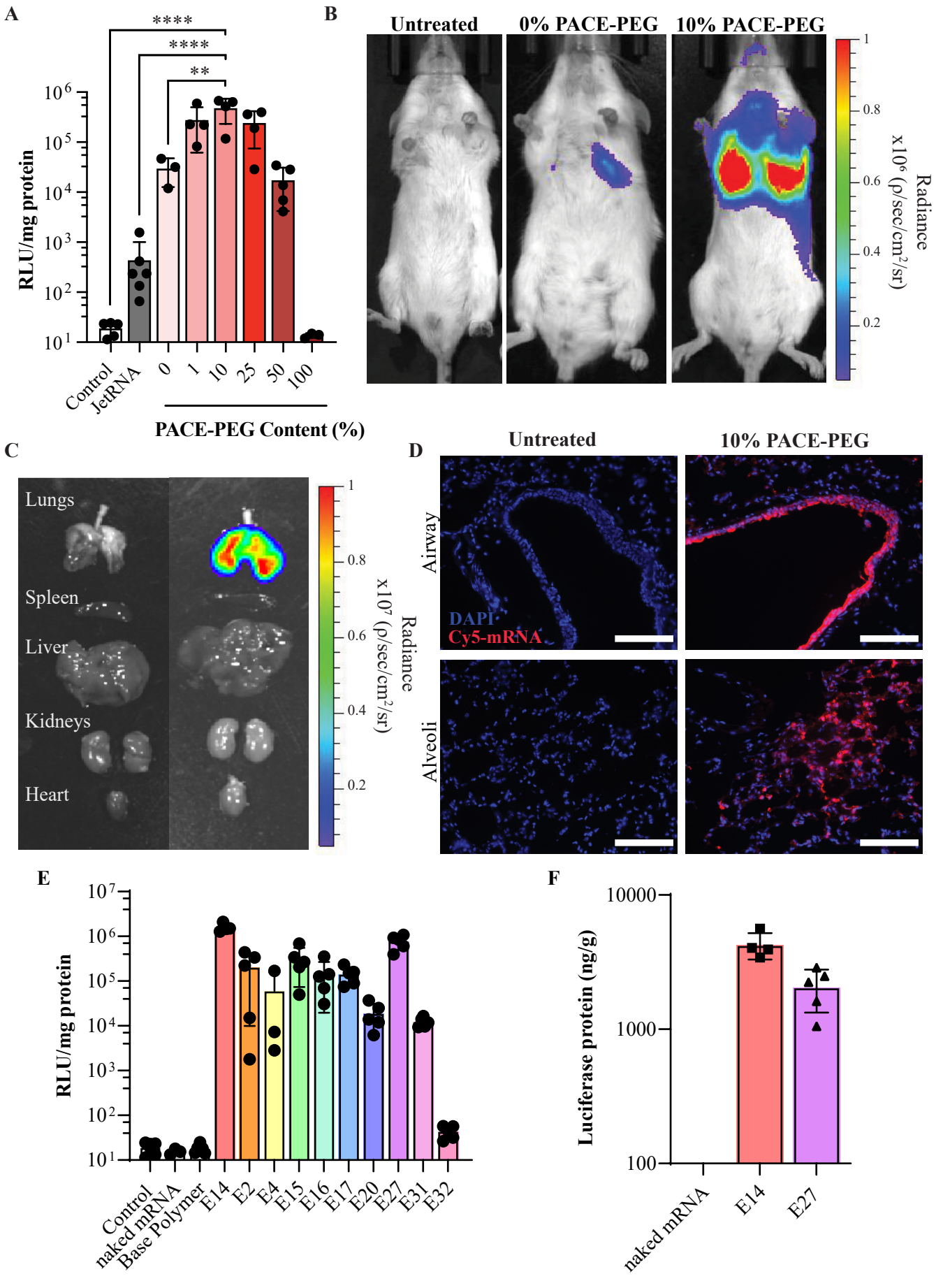
A
****
****
**
RLU/mg protein
Control
JetRNA
0
1
10
25
50
100
PACE-PEG Content (%)
B
Untreated
0% PACE-PEG
10% PACE-PEG
Radiance
x10⁶ (p/sec/cm²/sr)
C
Lungs
Spleen
Liver
Kidneys
Heart
Radiance
x10⁷ (p/sec/cm²/sr)
D
Untreated
10% PACE-PEG
Airway
Alveoli
DAPI
Cy5-mRNA
E
RLU/mg protein
Control
naked mRNA
Base Polymer
E14
E2
E4
E15
E16
E17
E20
E27
E31
E32
F
Luciferase protein (ng/g)
naked mRNA
E14
E27

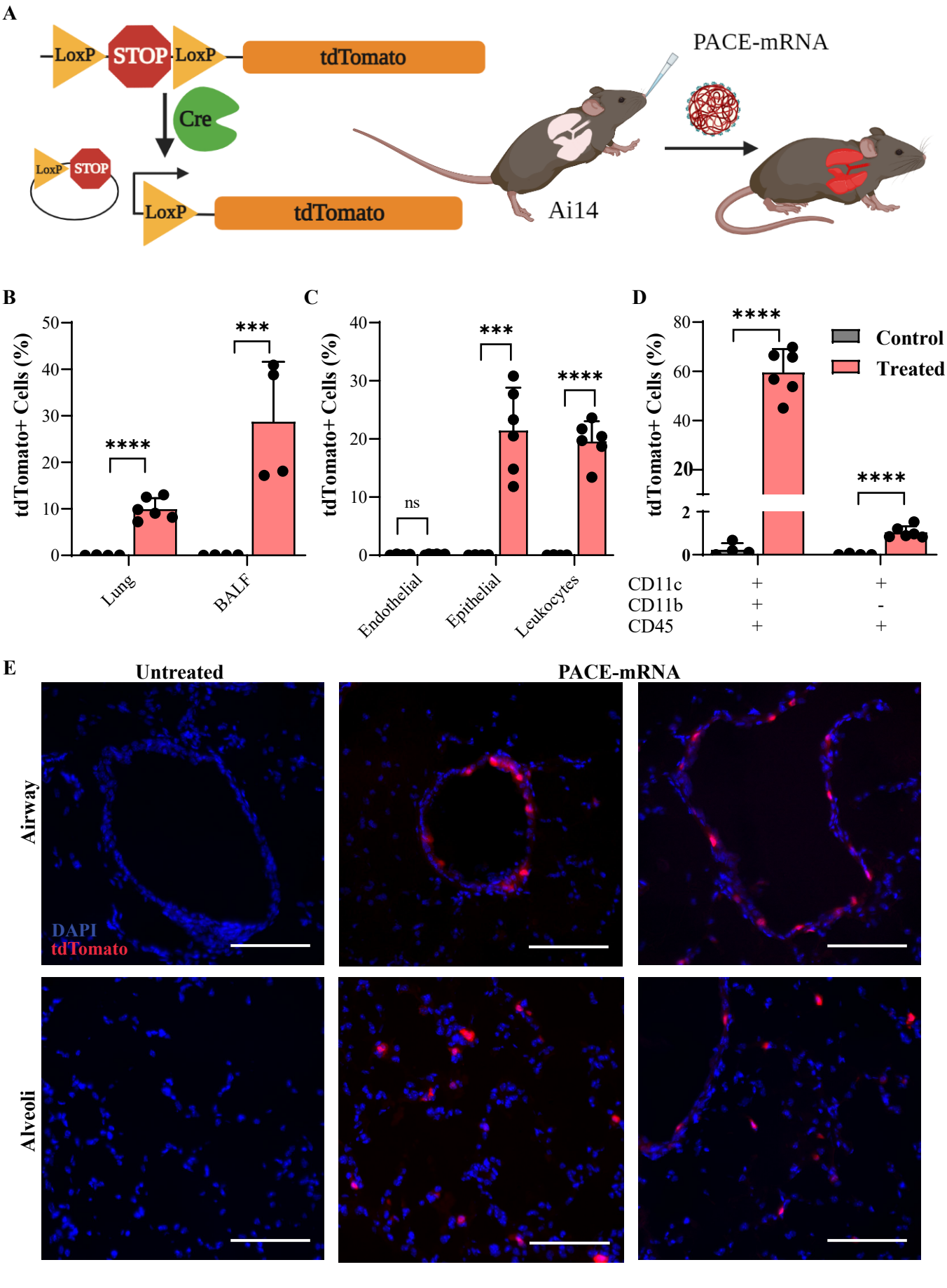
A
LoxP
STOP
LoxP
tdTomato
Cre
LoxP
STOP
LoxP
tdTomato
Ai14
PACE-mRNA
B
tdTomato+ Cells (%)
50
40
30
20
10
0
****
***
Lung
BALF
C
tdTomato+ Cells (%)
40
30
20
10
0
ns
***
****
Endothelial
Epithelial
Leukocytes
D
tdTomato+ Cells (%)
80
60
40
20
2
0
****
****
Control
Treated
CD11c + +
CD11b + -
CD45 + +
E
Untreated
PACE-mRNA
Airway
Alveoli
DAPI
tdTomato

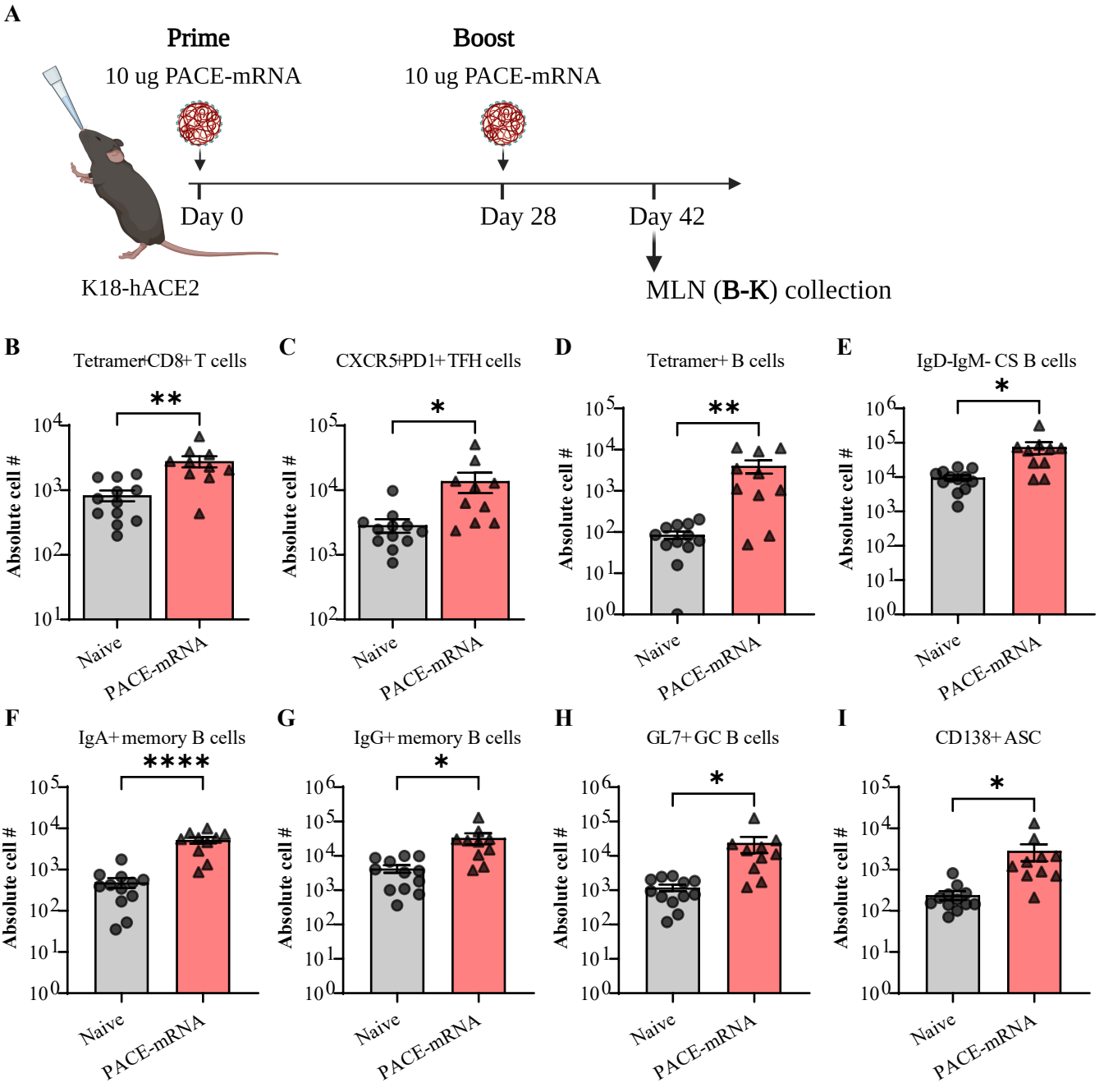
A
Prime
10 ug PACE-mRNA
Boost
10 ug PACE-mRNA
Day 0
Day 28
Day 42
K18-hACE2
MLN (B-K) collection
B
Tetramer+CD8+ T cells
C
CXCR5+PD1+ TFH cells
D
Tetramer+ B cells
E
IgD-IgM- CS B cells
F
IgA+ memory B cells
G
IgG+ memory B cells
H
GL7+ GC B cells
I
CD138+ ASC
Absolute cell #
Naive
PACE-mRNA

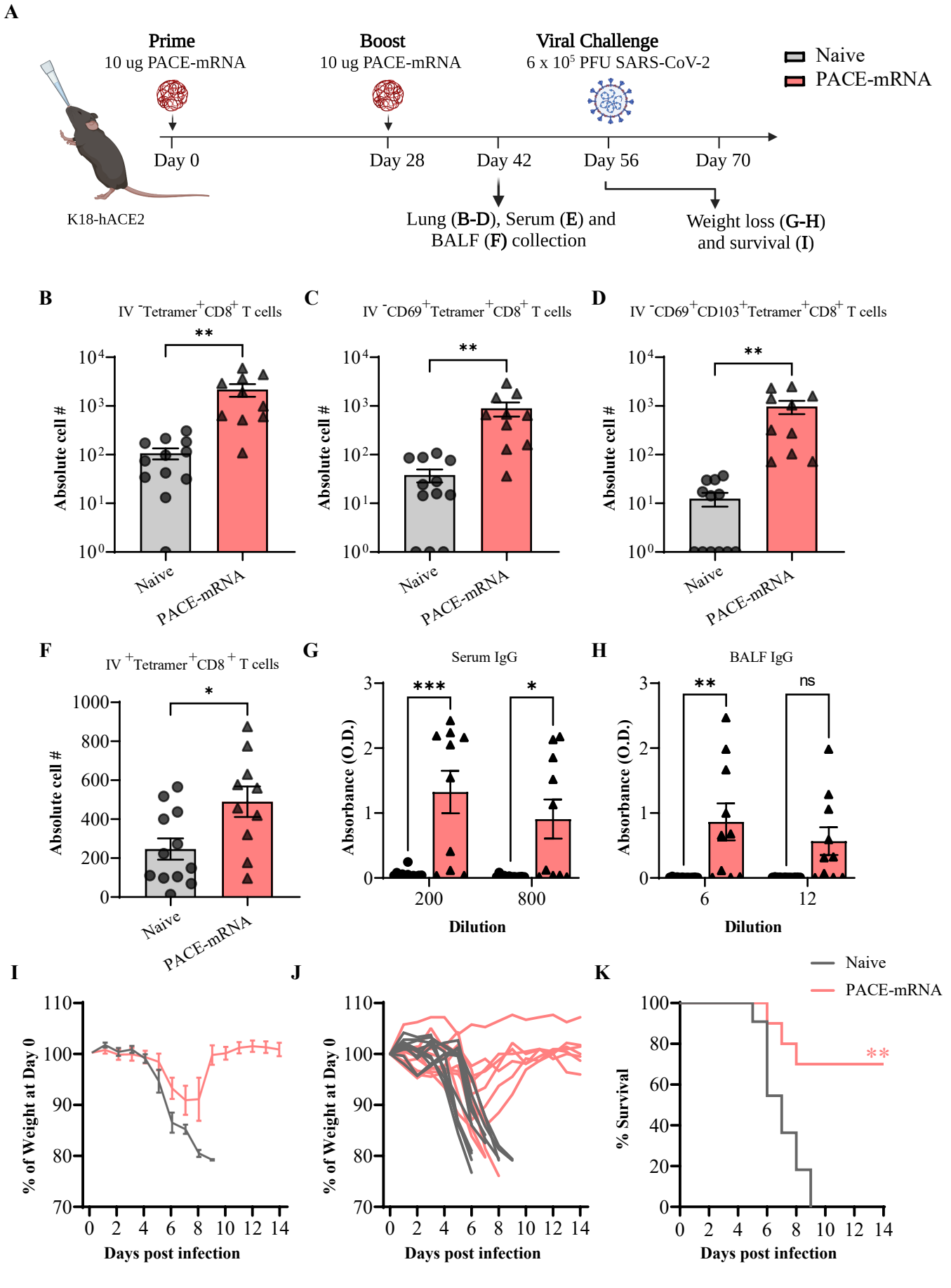
A
Prime
10 ug PACE-mRNA
Boost
10 ug PACE-mRNA
Viral Challenge
6 x 10^5 PFU SARS-CoV-2
Naive
PACE-mRNA
Day 0
Day 28
Day 42
Day 56
Day 70
K18-hACE2
Lung (B-D), Serum (E) and BALF (F) collection
Weight loss (G-H) and survival (I)
B
IV -Tetramer+CD8+ T cells
C
IV -CD69+Tetramer+CD8+ T cells
D
IV -CD69+CD103+Tetramer+CD8+ T cells
Absolute cell #
Naive
PACE-mRNA
F
IV +Tetramer+CD8+ T cells
G
Serum IgG
H
BALF IgG
Absorbance (O.D.)
Dilution
ns
I
J
K
% of Weight at Day 0
Days post infection
% Survival